Some Aspects of Autonomous Robot Navigation with Unscented HybridSLAM

Amir Monjazeb[1], Jurek Z. Sasiadek [1] and Dan Necsulescu[2]
[1]Department of Mechanical and Aerospace Engineering, Carleton University, 1125 Colonel By Drive, Ottawa, Canada
[2]Department of Mechanical Engineering, Ottawa University, 161 Louis Pasteur, CBY A205, Ottawa, Canada

Keywords: Simultaneous Localization And Mapping (SLAM) Problem, EKF, FastSLAM, HybridSLAM, Unscented HybridSLAM, Cluttered Environment, Double Loop Closing, Absolute Error.

Abstract: This paper addresses the linearization process of an autonomous mobile robot utilizing the second order Sterling polynomial interpolation specifically used for Unscented HybridSLAM algorithm. It describes the implementation of the linearization method to estimate the posterior mean and covariance of the system. The major interest is to apply linearized equations for a simultaneous localization and mapping case in a non-domestic environment with a random distribution of landmarks. Using computer simulations, Unscented HybridSLAM and the associated theoretical interpolation is examined for a double-loop scenario and the efficacy of the Unscented HybridSLAM is validated.

1 INTRODUCTION

The main task of a feature-based SLAM algorithm is to estimate the path of the robot and map of the environment as accurate as possible. There are many methods in which the robot uses different sensors to measure positions of landmarks as well as pose of the robot (Williams et al., 2002). Sensor readings are analyzed in these methods to extract data from the active or passive features in the environment to match it with a-priori known information in order to determine the current position of the robot. Usually, the task of extracting and matching data with a-priori information is easy for a domestic environment in which landmarks are distributed evenly. If the robot has a notation of evenly distribution of landmarks, the extracting of such data would be rather easier. For some SLAM cases in which the robot is equipped with restricted sensors, a uniform distribution of landmarks would considerably reduce the ambiguity of data association in the environment (Sasiadek et al., 2008). The advantage in such cases would be the elimination of data extracted from wrongly observed landmarks. Since the robot is aware of a uniform set of landmarks, sensor readings that result more than a specific threshold would be automatically deleted from the estimation process as a result of the Maximum Likelihood Rule (Thrun et al., 2004).

2 STERLING POLYNOMIAL INTERPOLATION

The formulation of the second order Sterling Polynomial Interpolation (SPI) is the basis of derivation of the Divided Deference Filter (DDF) and the Central Difference Filter (CDF) (Norgard et al., 2000). To formulate the equations of the system in a linear form, the second order SPI will be discussed in this section to indicate how a non-linear system can be approximated in a linear form. Then, the mean and covariance of the system in the posterior state will be discussed. Based on Taylor series of a non-linear function in [5], a random variable x around a statistical point $\bar{x}$ as its mean, can be expressed by

$$h(x) = h(\bar{x}) + D_{\delta_x} h + \frac{1}{2!} D_{\delta_x}^2 h + \cdots = h(\bar{x}) + (x-\bar{x})\frac{dh(x)}{dx} + \frac{1}{2!}(x-\bar{x})^2 \frac{d^2 h(x)}{dx^2} \quad (1)$$

The SPI formula (Julier, Uhlmann, 2004) uses a finite number of functional evaluations to approximate the above non-linear function with $\tilde{D}_{\Delta_x}$ as the first and $\tilde{D}_{\Delta_x}^2$ as the second order central divided difference operators acting on h(x), ℓ is the interval length or central difference step size and

Monjazeb A., Z. Sasiadek J. and Necsulescu D..
Some Aspects of Autonomous Robot Navigation with Unscented HybridSLAM.
DOI: 10.5220/0004452700660073
In *Proceedings of the 10th International Conference on Informatics in Control, Automation and Robotics* (ICINCO-2013), pages 66-73
ISBN: 978-989-8565-71-6

$\bar{x}$ is the prior mean of x around which the expansion is done. The resulting formula can be expressed as

$$h(x) = h(\bar{x}) + \tilde{D}_{\Delta_x} h + \frac{1}{2!}\tilde{D}^2_{\Delta_x} h \quad (2)$$

$$\tilde{D}_{\Delta_x} = (x - \bar{x})\frac{h(\bar{x}+\ell) - h(\bar{x}-\ell)}{2\ell} \quad (3)$$

$$\tilde{D}^2_{\Delta_x} = (x-\bar{x})^2 \frac{h(\bar{x}+\ell) + h(\bar{x}-\ell) - 2h(\bar{x})}{\ell^2} \quad (4)$$

In some cases (Dahlquist and Bjorck, 1974), the SPI formula can be interpreted as the Taylor series. If this formula is extended to the multi dimensional case, the function *h(**x**)* may be obtained by first stochastically decoupling the prior random variable *x* by the linear transformation as

$$\mathbf{y} = \mathbf{S}_x^{-1}\mathbf{x} \quad (5)$$

$$\tilde{h}(\mathbf{y}) = h(\mathbf{S}_x \mathbf{y}) = h(\mathbf{x}) \quad (6)$$

where $\mathbf{S}_x$ is called Cholesky factor (Smith, Self, and Cheesman, 1974) of the covariance matrix P_x of x such that $P_x = S_x S_x^T$. It should be noted that Taylor series expansion of $h(.)$ and $\tilde{h}(.)$ is identical if the expected value of vector x is E[x] and the covariance of the system is the expected value of P_x = $E[(\mathbf{x}-\bar{\mathbf{x}})(\mathbf{x}-\bar{\mathbf{x}})^T]$, the transformation stochastically decouples variables in **x** so that the interval components of **y** becomes mutually uncorrelated.

$$\mathbf{P}_y = E[(\mathbf{y}-\bar{\mathbf{y}})(\mathbf{y}-\bar{\mathbf{y}})^T] = \mathbf{I} \quad (7)$$

Assuming that L is the dimension of **x** and **y** with $\Delta_{y_i} = (\mathbf{y}-\bar{\mathbf{y}})_i$ as the i^{th} component of $\mathbf{y}-\bar{\mathbf{y}}$ (i= 1, … , L), $\boldsymbol{e}_i$ is the i^{th} unit vector, $\boldsymbol{d}_i$ is the partial first order difference, $\boldsymbol{d}_i^2$ is the partial second order difference, and $\boldsymbol{m}_i$ is the mean operator (Monjazeb et al. , 2012). Therefore,

$$\tilde{\mathbf{D}}_{\Delta_y}\tilde{h} = \left(\sum_{i=1}^{L}\Delta_{y_i}\boldsymbol{m}_i\boldsymbol{d}_i\right)\tilde{h}(\bar{\mathbf{y}}) \quad (8)$$

$$\tilde{\mathbf{D}}^2_{\Delta_y}\tilde{h} = \left(\sum_{i=1}^{L}\Delta^2_{y_i}\boldsymbol{d}_i^2 + \sum_{j=1}^{L}\sum_{q=1}^{L}\Delta_{y_j}\Delta_{yq}(\boldsymbol{m}_j\boldsymbol{d}_j)(\boldsymbol{m}_q\boldsymbol{d}_q)\right)\tilde{h}(\bar{\mathbf{y}}) \quad (9)$$

$$\boldsymbol{d}_i\tilde{h}(\bar{\mathbf{y}}) = \frac{1}{2\ell}\left[\tilde{h}(\bar{\mathbf{y}} + \ell\mathbf{e}_i) - \tilde{h}(\bar{\mathbf{y}} - \ell\mathbf{e}_i)\right] \quad (10)$$

$$\boldsymbol{d}_i^2\tilde{h}(\bar{\mathbf{y}}) = \frac{1}{2\ell^2}\left[\tilde{h}(\bar{\mathbf{y}}+\ell\mathbf{e}_i) + \tilde{h}(\bar{\mathbf{y}}-\ell\mathbf{e}_i) - 2\tilde{h}(\bar{\mathbf{y}})\right] \quad (11)$$

$$\boldsymbol{m}_i\tilde{h}(\bar{\mathbf{y}}) = \frac{1}{2}\left[\tilde{h}(\bar{\mathbf{y}} + \ell\mathbf{e}_i) + \tilde{h}(\bar{\mathbf{y}} - \ell\mathbf{e}_i)\right] \quad (12)$$

using equations (5) and (6) and considering that s_{x_i} is the i^{th} column of the Cholesky factor of covariance matrix of **x** we can induce

$$\begin{aligned}\tilde{h}(\bar{\mathbf{y}} \pm \ell\mathbf{e}_i) &= h(\mathbf{S}_x[\bar{\mathbf{y}} \pm \ell\mathbf{e}_i] \\ &= h(\mathbf{S}_x\bar{\mathbf{y}} \pm \ell\mathbf{S}_x\mathbf{e}_i) = h(\bar{\mathbf{x}} \pm \ell s_{x_i})\end{aligned} \quad (13)$$

$$s_{x_i} = \mathbf{S}_x\mathbf{e}_i = (\mathbf{S}_x)_i = (\sqrt{\mathbf{P}_x})_i \quad (14)$$

Set of vectors defined in equation (13) is equivalent so that that the UKF generates its set of sigma-points with only the difference in the value of the weighting term (Julier and Uhlmann, 2001).

3 POSTERIOR MEAN AND COVARIANCE ESTIMATION

The observation function can be expressed through a non-linear function *h(.)* and with considering non-linear transformation of an L dimensional random variable **x** with covariance $\mathbf{P}_x$ and mean $\bar{\mathbf{x}}$ as follows

$$\mathbf{z}_k = h(\mathbf{x}_k) = \tilde{h}(\mathbf{y}_k) \approx \tilde{h}(\mathbf{y}_k) + \tilde{\mathbf{D}}_{\Delta_y}\tilde{h} + \frac{1}{2}\tilde{\mathbf{D}}^2_{\Delta_y}\tilde{h} \quad (15)$$

$$\mathbf{y} = \mathbf{S}_x\mathbf{x} \quad (16)$$

The posterior mean of $\mathbf{y}$ and its covariance and cross covariance are defined as

$$\bar{\mathbf{z}}_k = E[\mathbf{z}_k] \quad (17)$$

$$\mathbf{P}_{z_k} = E[(\mathbf{z}_k - \bar{\mathbf{z}}_k)(\mathbf{z}_k - \bar{\mathbf{z}}_k)^T] \quad (18)$$

$$\mathbf{P}_{x_k z_k} = E[(\mathbf{x}_k - \bar{\mathbf{x}}_k)(\mathbf{z}_k - \bar{\mathbf{z}}_k)^T] \quad (19)$$

Assuming that $\Delta_y = (\mathbf{y}-\bar{\mathbf{y}})$ is a zero-mean unity variance random variable which is symmetric (Norgard et al., 2000) as defined in equation (5), the mean is approximated as

$$\bar{\mathbf{z}}_k \approx E[\tilde{h}(\mathbf{y}_k) + \tilde{\mathbf{D}}_{\Delta_y}\tilde{h} + \frac{1}{2}\tilde{\mathbf{D}}^2_{\Delta_y}\tilde{h}] \quad (20)$$

$$= \tilde{h}(\mathbf{y}_k) + E[\frac{1}{2}\tilde{\mathbf{D}}^2_{\Delta_y}\tilde{h}] \quad (21)$$

$$= \tilde{h}(\mathbf{y}_k) + E\left[\frac{1}{2\ell^2}\left(\sum_{i=1}^{L}\Delta^2_{y_i}\boldsymbol{d}_i^2\right)\tilde{h}(\mathbf{y}_k)\right] \quad (22)$$

$$= \tilde{h}(\mathbf{y}_k) + \frac{1}{2\ell^2}\sum_{i=1}^{L}[\tilde{h}(\bar{\mathbf{y}}_k + \ell\mathbf{e}_i) + \tilde{h}(\bar{\mathbf{y}}_k - \ell\mathbf{e}_i) - 2\tilde{h}(\mathbf{y}_k)] \quad (23)$$

$$= \frac{\ell^2 - L}{\ell^2}\tilde{h}(\mathbf{y}_k) + \frac{1}{2\ell^2}\sum_{i=1}^{L}[\tilde{h}(\bar{\mathbf{y}}_k + \ell\mathbf{e}_i) + \tilde{h}(\bar{\mathbf{y}}_k - \ell\mathbf{e}_i)] \quad (24)$$

By rewriting the posterior mean in terms of motion vector (Brooks and Bailey, 2009) we will have

$$\bar{\mathbf{z}}_k = \frac{\ell^2 - L}{\ell^2}\tilde{h}(\mathbf{x}_k) + \frac{1}{2\ell^2}\sum_{i=1}^{L}[\tilde{h}(\bar{\mathbf{x}}_k + \ell s_{x_i}) + \tilde{h}(\bar{\mathbf{y}}_k - \ell s_{x_i})] \quad (25)$$

Using the identity

$$\begin{aligned}\bar{\mathbf{z}}_k &= \mathrm{E}[\mathbf{z}_k] = \mathrm{E}[\mathbf{z}_k] + h(\bar{\mathbf{x}}_k) - h(\bar{\mathbf{x}}_k) \\ &= \mathrm{E}[\mathbf{z}_k] + h(\bar{\mathbf{x}}_k) - \mathrm{E}[h(\bar{\mathbf{x}}_k)] \\ &= h(\bar{\mathbf{x}}_k) + \mathrm{E}[\mathbf{z}_k - h(\bar{\mathbf{x}}_k)]\end{aligned} \quad (26)$$

$$\begin{aligned}\mathbf{P}_{z_k} &= \mathrm{E}[(\mathbf{z}_k - \bar{\mathbf{z}}_k)(\mathbf{z}_k - \bar{\mathbf{z}}_k)^T] \\ &= \mathrm{E}[(\mathbf{z}_k - h(\mathbf{x}_k))(\mathbf{z}_k - h(\mathbf{x}_k))^T] \\ &\quad - \mathrm{E}[(\mathbf{z}_k - h(\mathbf{x}_k))]\mathrm{E}[(\mathbf{z}_k - h(\mathbf{x}_k))]^T \\ &= \mathrm{E}[(\mathbf{z}_k - \tilde{h}(\mathbf{y}_k))(\mathbf{z}_k - \tilde{h}(\mathbf{y}_k))^T] \\ &\quad - \mathrm{E}[(\mathbf{z}_k - \tilde{h}(\mathbf{y}_k))]\mathrm{E}[(\mathbf{z}_k - \tilde{h}(\mathbf{y}_k))]^T\end{aligned} \quad (27)$$

From equation (15), the second order approximation of $\mathbf{z}_k - \tilde{h}(\mathbf{y}_k) = \tilde{\mathbf{D}}_{\Delta_y}\tilde{h} + \frac{1}{2}\tilde{\mathbf{D}}^2_{\Delta_y}\tilde{h}$ can be substituted into equation (27) and therefore,

$$\begin{aligned}\mathbf{P}_{z_k} \approx\ & \mathrm{E}[(\tilde{\mathbf{D}}_{\Delta_y}\tilde{h} + \tfrac{1}{2}\tilde{\mathbf{D}}^2_{\Delta_y}\tilde{h}) \\ & \times(\tilde{\mathbf{D}}_{\Delta_y}\tilde{h} + \tfrac{1}{2}\tilde{\mathbf{D}}^2_{\Delta_y}\tilde{h})^T] \\ & -\mathrm{E}[(\tilde{\mathbf{D}}_{\Delta_y}\tilde{h} + \tfrac{1}{2}\tilde{\mathbf{D}}^2_{\Delta_y}\tilde{h})] \\ & \times\mathrm{E}[(\tilde{\mathbf{D}}_{\Delta_y}\tilde{h} + \tfrac{1}{2}\tilde{\mathbf{D}}^2_{\Delta_y}\tilde{h})]^T\end{aligned} \quad (28)$$

$\Delta_y = (\mathbf{y} - \bar{\mathbf{y}})$ is symmetric, therefore, all resulting odd-order expected moments have zero value. Since the number of terms in this calculation grows rapidly with the dimension of **y,** the inclusion of such terms leads the computation highly complex. As a result all components of the resulting fourth order term, $\mathrm{E}[\frac{1}{4}(\tilde{\mathbf{D}}^2_{\Delta_y}\tilde{h})(\tilde{\mathbf{D}}^2_{\Delta_y}\tilde{h})^T]$, that contains cross differences in the expansion of equation (28) are discarded. The extra effort worthwhile is not considered since it is not possible to capture all fourth order moments (Monjazeb, Sasiadek, and Necsulescu, 2011). The approximation of the covariance and cross-covariance matrices are expressed as below. For the details refer to (Norgard et al., 2000).

In equation (30) the odd-order moment terms are all zero since $(\mathbf{y}_k - \bar{\mathbf{y}}_k)$ is symmetric. The optimal setting of the central difference interval parameter, ℓ, is dictated by the prior distribution of $\mathbf{y} = \mathbf{S}_x^{-1}\mathbf{x}$. For Gaussian priors, the optimal value of h is thus $h = \sqrt{3}$. For more details see (Norgard et al., 2000).

$$\begin{aligned}\mathbf{P}_{z_k} \approx\ & \frac{1}{4\ell^2}\sum_{i=1}^{L}[h(\bar{\mathbf{x}}_k + \ell s_{x_i}) - h(\bar{\mathbf{x}}_k - \ell s_{x_i})] \\ & \times[h(\bar{\mathbf{x}}_k + \ell s_{x_i}) - h(\bar{\mathbf{x}}_k - \ell s_{x_i})]^T \\ & + \frac{\ell^2 - 1}{4\ell^4}\sum_{i=1}^{L}[\\ & [h(\bar{\mathbf{x}}_k + \ell s_{x_i}) + h(\bar{\mathbf{x}}_k - \ell s_{x_i}) - 2h(\bar{\mathbf{x}}_k)] \times \\ & [h(\bar{\mathbf{x}}_k + \ell s_{x_i}) + h(\bar{\mathbf{x}}_k - \ell s_{x_i}) - 2h(\bar{\mathbf{x}}_k)]^T]\end{aligned} \quad (29)$$

$$\begin{aligned}\mathbf{P}_{x_k z_k} &= \mathrm{E}[(\mathbf{x}_k - \bar{\mathbf{x}}_k)(\mathbf{z}_k - \bar{\mathbf{z}}_k)^T] \\ &\approx \mathrm{E}[(\mathbf{S}_x(\mathbf{y}_k - \bar{\mathbf{y}}_k)[\tilde{\mathbf{D}}_{\Delta_y}\tilde{h} + \tfrac{1}{2}\tilde{\mathbf{D}}^2_{\Delta_y}\tilde{h} - \mathrm{E}[\\ &\quad \tfrac{1}{2}\tilde{\mathbf{D}}^2_{\Delta_y}\tilde{h}]]^T] = \mathrm{E}[(\mathbf{S}_x(\mathbf{y}_k - \bar{\mathbf{y}}_k)[\tilde{\mathbf{D}}_{\Delta_y}\tilde{h}]^T] \\ &\quad + \tfrac{1}{2}\mathrm{E}[(\mathbf{S}_x(\mathbf{y}_k - \bar{\mathbf{y}}_k)[\tilde{\mathbf{D}}^2_{\Delta_y}\tilde{h}]^T] \\ &\quad - \tfrac{1}{2}\mathrm{E}[(\mathbf{S}_x(\mathbf{y}_k - \bar{\mathbf{y}}_k)] \times \mathrm{E}[\tfrac{1}{2}\tilde{\mathbf{D}}^2_{\Delta_y}\tilde{h}]^2\end{aligned} \quad (30)$$

$$= \mathrm{E}[(\mathbf{S}_x(\mathbf{y}_k - \bar{\mathbf{y}}_k)[\tilde{\mathbf{D}}_{\Delta_y}\tilde{h}]^T] \quad (31)$$

$$= \frac{1}{2\ell}\sum_{i=1}^{L}\mathbf{s}_{x_i}[\tilde{h}(\bar{\mathbf{y}}_k + \ell\mathbf{e}_i) - \tilde{h}(\bar{\mathbf{y}}_k - \ell\mathbf{e}_i)]^T \quad (32)$$

$$= \frac{1}{2\ell}\sum_{i=1}^{L}\mathbf{s}_{x_i}[h(\mathbf{x}_k + \ell\mathbf{s}_{x_i}) - h(\mathbf{x}_k - \ell\mathbf{s}_{x_i})]^T \quad (33)$$

4 SIMULATIONS AND RESULTS

4.1 Landmark Estimation Threshold

Figure 1-a shows a path in an environment with a

non-uniform distribution of landmarks. Figure 1-b depicts the range of position estimation of landmark at x=30m and y=20m. The error in this case indicates that the estimated location of the landmark is within ±0.40m. In this particular scenario, the level of data ambiguity does not arise exponentially when the distribution of landmarks change from uniform to random. Figure 2 compares the ambiguity of data with the use of EKF-SLAM as well as using 3000 particles resulted by FastSLAM, HybridSLAM, and Unscented HybridSLAM. Hundreds of dots that make different formations around in the range are depicted in this figure for each specific algorithm. The threshold range (oval) is obtained using a standard EKF under Gaussian conditions. The true position of the landmark is at x=30m and y=20m. The banana shape in figure 2-a, shows the estimation result using the first order Taylor series in EKF under non-Gaussian conditions which appears to be highly inaccurate.

The banana shape in figure 2-b, illustrates a reduction of error in the location estimation of the landmark using FastSLAM and as a result less ambiguity in data. However, estimated points do not fit in the standard oval and there are about 60% of estimated points off the standard threshold. HybridSLAM has relatively less ambiguity in data association as shown in figure 2-c. As shown in the picture, there are only 30% of points outside the range. Moreover, the estimation dots are mostly inside the standard range. Nonetheless, it is still far from the standard threshold and may not be an acceptable result for SLAM applications. The estimation of the landmark with Unscented Kalman Filter creates an oval shape around the true location of the landmark and is the one with the least ambiguity in data association. As demonstrated in figure 2-d, about 15% of estimated points are outside the standard range which proves that HS has the most acceptable result amongst all other algorithms. As a result, UHS is the only algorithm which is a recursive filter based on sterling approximation and has the least tendency to diverge. Figures 3 to 5 demonstrate the performance of Unscented HybridSLAM for the scenario depicted in figure 1. In figure 5 the location estimation error of landmark (x=10, y=0) is approximately 0.2m. In figure 6 the error of location estimation of landmark (x=30, y=40) is approximately 0.25m.

4.2 Double Loop Closing Scenario

In this section, simulation results of a double loop

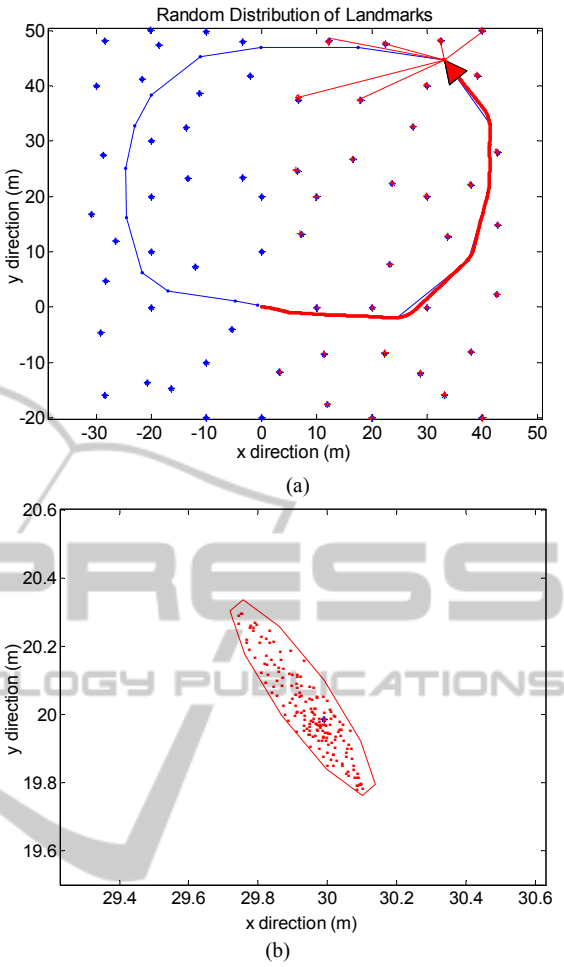

Figure 1: Random Distribution of Landmarks a) non-uniform distribution of landmarks in the environment. b) estimated position of the landmark located at (x=30, y=20).

scenario using Unscented HybridSLAM algorithm are presented. Here, the double loop closing case is exemplified in order to analyze the performance of the algorithm while the robot is travelling across more complex terrain. Figure 7 shows a map of the environment that contains an uneven distribution of landmarks. The figure also shows the true path of the robot. The speed of the mobile robot is assumed 3.5 m/s. The robot completes the whole loop in approximately 2800 seconds. Number of particles used in this experiment is 500. In figure 7 the true map of the environment and observation results before closing the loop are depicted. The vehicle starts at the centre of the test area (x=0, y=0) and travels counter clock wise. During the navigation process landmarks are observed and the uncertainty increases slightly. The uncertainty in the

observations is at the largest value on the third part of path. Figure 8 demonstrates the actual error and standard deviations of the process when the robot is at the third part of the path. Simulation results illustrate the actual location error along x and y axes respectively. Dashed lines represent the 1-sigma estimated uncertainty. The simulated result indicates that UHS is a consistent method with the actual error.

Figure 9 shows the evolution of the uncertainty for 4 out of 6 landmarks located in the smaller loop at the beginning of the process. All solid lines represent the deviations and dashed lines represent the location estimation error. Comparing the error between actual landmarks positions and those estimated with the 2-sigma deviations indicate that the UHS algorithm is consistent, specifically with respect to landmarks location error. As expected, the actual landmarks error and uncertainty have been reduced. Two out of six landmarks were not observed due to the scanner range limitations. Figure 10 shows the result in regard to the orientation deviation and absolute error right after the loop is closed and indicates that the map becomes more correlated at the end of the first run. Figure 11 depicts the situation in which the loop is closed and the robot is at one third of the path again. The robot is at point (x=-20, y=34) and heading to complete the second loop. The uncertainty in the observation of landmarks at this point is considerably reduced, meaning that the outcome of loop closing is successful and the filter converges. Moreover, all observable landmarks have been estimated correctly following the completion of the first run. Figure 12 demonstrates absolute error and deviations along x and y axes, the orientation, and for six landmarks inside the internal loop after the robot completes the loop and is at one third of its path during completion of the second loop. The evolution of the uncertainty for all six landmarks in the map indicate that the map correlation in maintained and leads the final map to be consistent. These results show that the estimated uncertainty is consistent with the actual error along both axes and the orientation of the vehicle. The orientation error is around 0.02 radians which confirms Unscented HybridSLAM algorithm consistency.

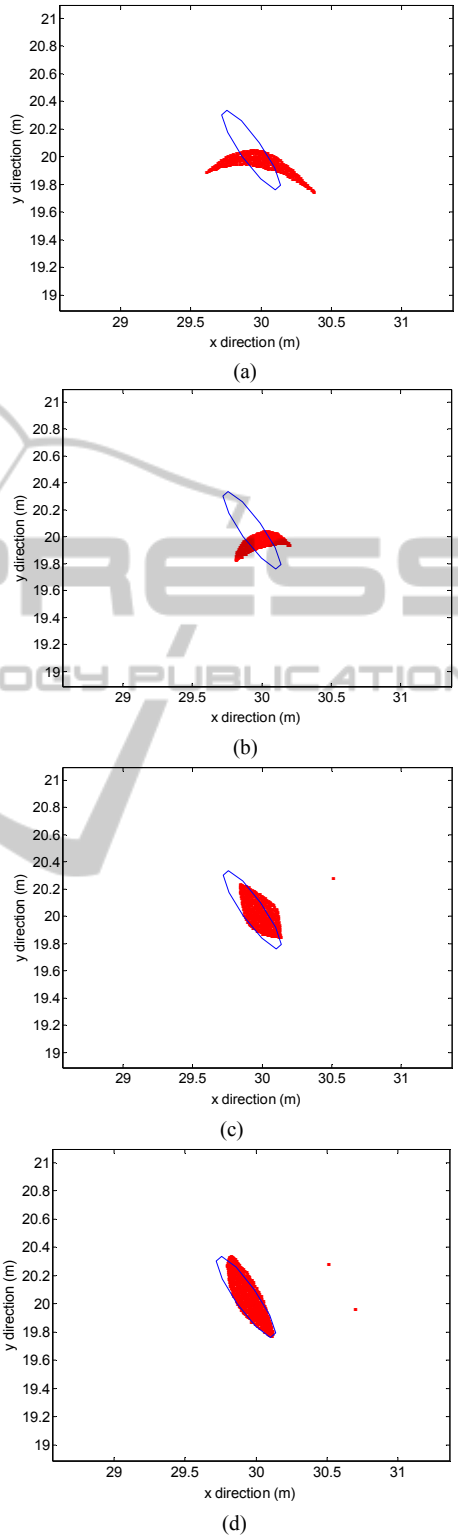

Figure 2: Estimated position of the landmarks a) EKF-SLAM under non-Gaussian conditions b) FastSLAM c) HybridSLAM d) Unscented HybridSLAM.

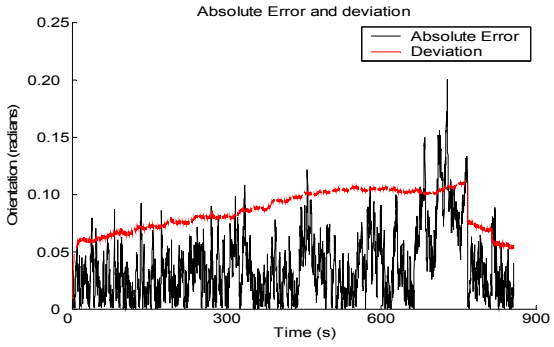

Figure 3: Orientation absolute error and deviation.

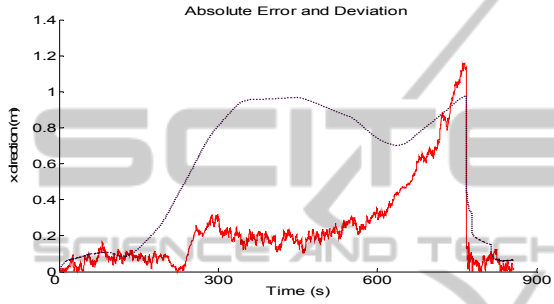

(a)

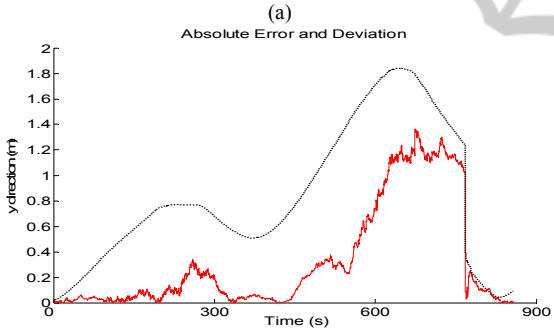

(b)

Figure 4: Deviation along a) x axis b) y axis.

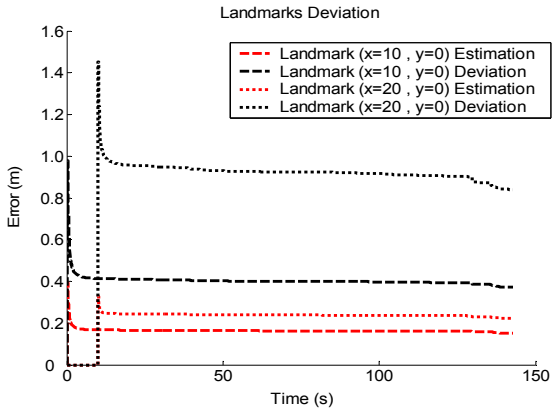

Figure 5: Landmarks deviation (x=10 , y=0) and (x=20 , y=0) using 3000 particles.

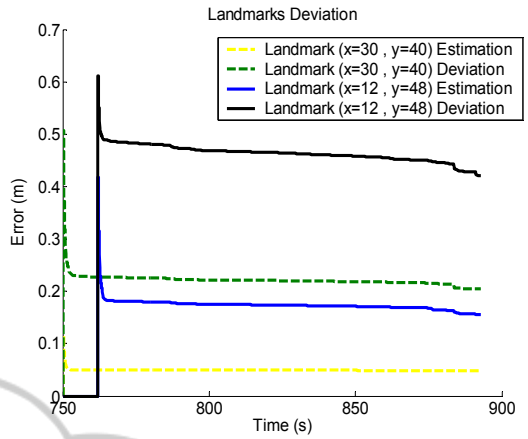

Figure 6: landmarks deviation (x=30 , y=40) and (x=12 , y=48) using 3000 particles.

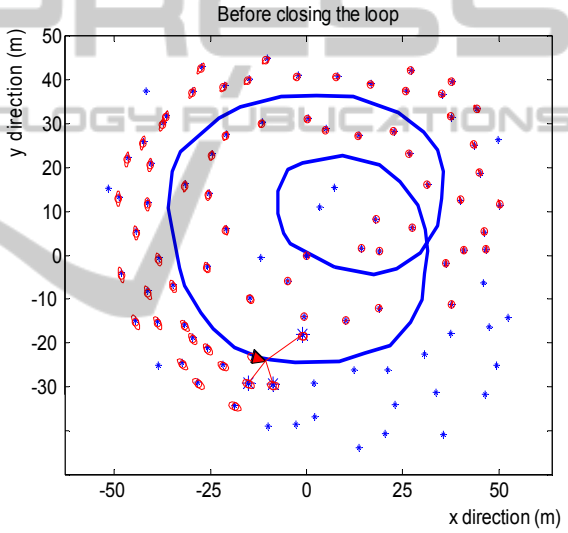

Figure 7: True map of the environment with 94 observable landmarks.

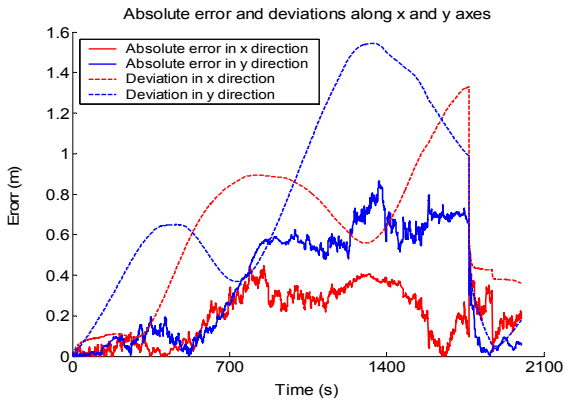

Figure 8: Absolute error and deviations.

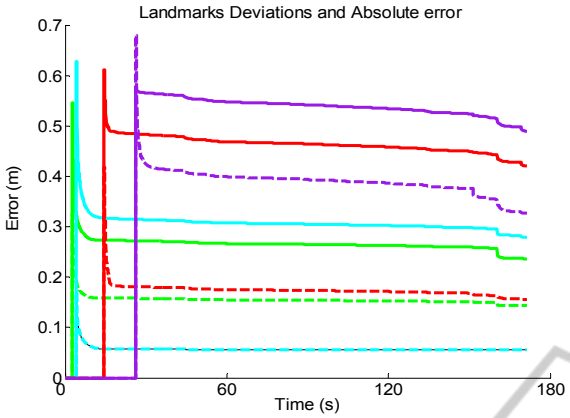

Figure 9: Landmark deviation and absolute error (a double loop case) using 500 particles.

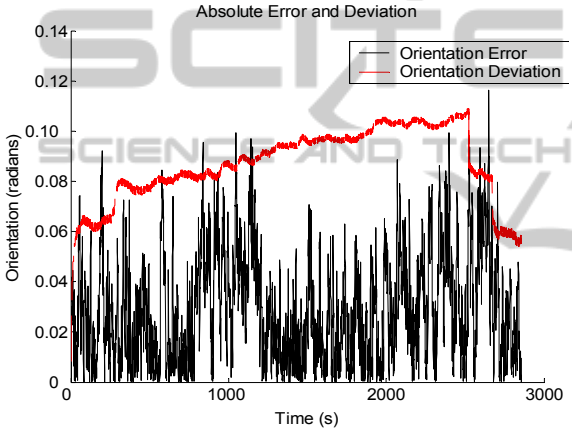

Figure 10: Orientation Absolute error and deviation (double loop case) using 500 particles.

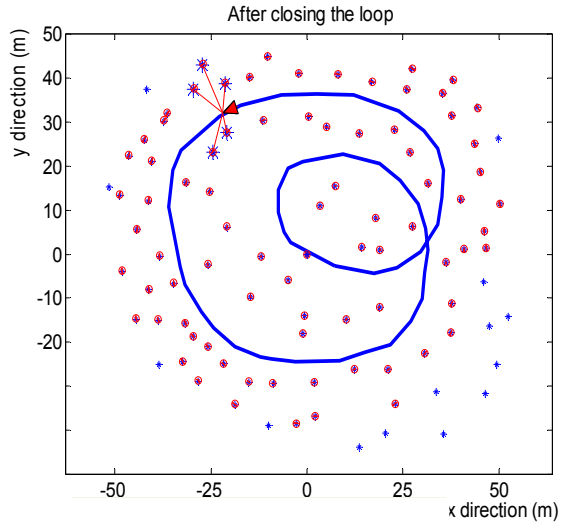

Figure 11: After the completion of the loop.

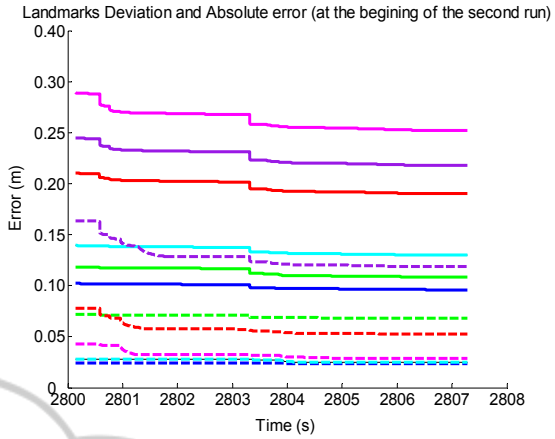

Figure 12: Landmark deviation after closing the loop.

6 CONCLUSIONS

The major shortcoming of most simultaneous localization and mapping algorithms is their limitation to the first order accuracy of propagated the mean and covariance as a result of first order truncated Taylor series linearization technique. Unscented HybridSLAM can address this issue with the use of a deterministic sampling approach to approximate the optimal gain and prediction terms in a linear Bayesian form. Unscented HybridSLAM, with its derivative-free Gaussian random variable propagation technique, is able to calculate the posterior mean and covariance of the system to the second order of Taylor series. In order to show how the model robot dynamics can be approximated, a derivative-free technique based on Sterling's polynomial interpolation formula was derived and presented in this paper. Derived equations were linearized due to the high non-linearity of the system. The second order Sterling Polynomial Interpolation was employed to approximate a non-linear function with first and second order central divided difference operators acting on the observation function expressed in a non-linear form. Simulation results indicated that with the second order Sterling polynomial linearization, Unscented HybridSLAM gained enough accuracy and stability in performance for double-loop scenarios in a non-domestic environment.

REFERENCES

Williams, S. B., Dissanayake, G., Durrant-Whyte, H., 2002, An Efficient Approach to the Simultaneous

Localisation and Mapping Problem", *Proceedings of the 2002 IEEE International Conference on Robotics & Automation*, Washington DC.

Thrun, S., Montemerlo, M., Koller, D., Wegbreit, B., Nieto, J., Nebot, E., 2004, FastSLAM: an efficient solution to the simultaneous localization and mapping problem with unknown data association, *Journal of Machine Learning Research*.

Norgard M., Poulsen N., Ravn O., 2000, *Advances in derivative-free state estimation for nonlinear systems*, Tech. Rep. IMM-REP, pp. 1998-2015, Dept. of Modelling, Technical University of Denmark..

Julier, S. J., Uhlmann, J. K., 2004, Unscented filtering and nonlinear estimation, *Proc. of IEEE Journal*, Vol. 92, Issue 3, pp. 401-422, March.

Dahlquist G., Bjorck A. Numerical methods, 1974, Prentice-Hall, NJ, Englewood Cliffs.

Smith R., Self M., Cheesman P., 1974, Estimating uncertain spatial relationships in robotics, Autonomous Robot Vehicles; *Coxand & Wilforn Ed.*, Springer Verlag, pp. 167-193.

Monjazeb, A., Sasiadek, J. Z., Necsulescu, D., 2012, Autonomous navigation of an outdoor mobile robot in a cluttered environment using a combination of unscented Kalman filter and a Rao-Blackwellised particle filter, 2012, *Proc. of 9th International Conference on Informatics in Control Automation and Robotics (ICINCO)*, pp. 485-488, Rome, Italy, July.

Monjazeb, A., Sasiadek, J. Z., Necsulescu, D., 2012, An approach to autonomous navigation based on Unscented HybridSLAM, *Proc. of 17th International Conference on Methods and Models in Automation and Robotics*, pp. 369-374, Miedzyzdroje, Poland.

Julier, S. J., Uhlmann, J. K., 2001, A counter example to the theory of simultaneous localization and map building, *Proc. of IEEE International Conference on Robotics and Automation*, pp. 4238-4243, March.

Brooks, A., Bailey, T., 2009, HybridSLAM: Combining FastSLAM and EKF-SLAM for reliable mapping, *Springer Tracts in Advanced Robotics*, Volume 57, pp. 647-661.

Norgard M., Poulsen N., Ravn O., 2000, New development in state estimation for nonlinear systems, *Journal of Automatica*, pp. 1627-1638, Vol. 36, No. 11, November.

Monjazeb, A., Sasiadek, J. Z., Necsulescu, D., Autonomous navigation among large number of nearby 2011, landmarks using FastSLAM and EKF-SLAM; a comparative study, *Proc. of 16th International Conference on Methods and Models in Automation and Robotics (MMAR)*, pp. 369-374, Miedzyzdroje, Poland.

Sasiadek, J. Z., Monjazeb, A., Necsulescu, D., 2008, Navigation of an autonomous mobile robot using EKF-SLAM and FastSLAM, *Proc. of 16th Mediterranean Conference on Control and Automation*, pp. 517-522, Ajaccio, France.